Applied Catalysis A: General 406 (2011) 34–42

Contents lists available at ScienceDirect

Applied Catalysis A: General

journal homepage: www.elsevier.com/locate/apcata

Structural changes occurring at the surface of alumina-supported nanoscaled Mo–V–Nb–(Te)–O catalytic system during the selective oxidation of propane to acrylic acid

Ricardo López-Medina[a], J.L.G. Fierro[b], M. Olga Guerrero-Pérez[c], M.A. Bañares[a,*]

[a] Catalytic Spectroscopy Laboratory, Instituto de Catálisis y Petroleoquímica, CSIC, Marie Curie, 2, E-28049-Madrid, Spain
[b] Energía y Química Sostenible, Instituto de Catálisis y Petroleoquímica, CSIC, Marie Curie, 2, E-28049-Madrid, Spain
[c] Departamento de Ingeniería Química, Universidad de Málaga, E-29071-Málaga, Spain

ARTICLE INFO

Article history:
Received 7 April 2011
Received in revised form 27 July 2011
Accepted 1 August 2011
Available online 10 August 2011

Keywords:
Operando Raman
Mo–V–Te–O
Acrylic acid
Structure–activity relationship
Support-stabilized nanoparticle
Nanostructured catalysts

ABSTRACT

The effect of total coverage on alumina is evaluated for $Mo_5V_4Nb_1/Al_2O_3$ catalysts by *operando* Raman-GC spectroscopy during reaction, demonstrating structural changes during reaction that do not occur during catalyst calcination. XRD detects show no appreciable change but *Operando* Raman-GC studies are sensitive to changes occurring in the nanometer scale, which modulate the performance during propane oxidation, delivering the structure–activity relationship for deactivation. Raman spectra confirm the formation of nanocrystalline MoO_3-type structures during reaction up to 375 °C, accompanied by coke deposits, able to block the active sites, being detrimental for the acrylic acid formation. Three new catalysts were preparing by the addition of tellurium as dopant, in this case, the presence of MoO_3 is not detected under reaction conditions, since the formation of a distorted rutile structure under reaction conditions is observed, and in this case acrylic acid is obtained as the main reaction product with a yield of ca. 25% at 400 °C.

1. Introduction

Industrial supported catalysts contain an active component, typically nanometer-sized particles of transition metals and oxides, which may be dispersed on a high-area support made of a relatively inert oxide [1]. Supported vanadium and molybdenum oxide catalysts represent an important class of catalysts which are industrially applied in oxidation reactions [2–4]; in particular, the selective oxidation of light alkanes over MoVNbTe mixed oxide catalysts has received much attention lately because of their industrial importance in the direct oxidation of propane to acrylic acid [5–9]; their performance is strongly affected by structural features. The addition of niobium and/or tellurium to vanadium and molybdenum oxides stabilizes the phases or mixed MoVNb oxide systems with high-performing selective oxidation catalytic properties, known as M1 and M2 phases [1–3]. In the absence of M1 and M2 phases, synergistic effects between nanocrystaline Mo_5O_{14} and an oxygen-defective MoO_{3-x} phase are proposed to account for the high catalytic performance of the multicomponent Mo–V–Nb oxide system [10]. Niobium is also efficient to stabilize nanosized MoO_{3-x} and $(VNbMo)_5O_{14}$ crystals [11].

Understanding the working state of a catalyst requires determining its structure and activity in a simultaneous fashion; *operando* analyses are particularly efficient to tackle this approach [12–18]. It is thus possible to characterize catalytic materials under reaction conditions, even at high temperatures, and assess structure–activity relationships [19,20]. Such information is the base for further progress and improvements on catalyst formulation and also to develop real-time spectroscopic control [21]. In a previous paper [22] we have reported how alumina-stabilized nanosized rutile Mo–V–Nb–(Te)–O oxide phases can be prepared and how such nanosized phases are efficient for the conversion of propane into acrylic acid. It has also been described [23] how the structure of these catalytic materials depends on calcination and reaction conditions, determining the catalytic behaviour. Thus, with the aim to uncover the changes occurring in the nanometer scale at the catalysts during reaction, the role of tellurium species, and to establish the relationships between the structure of catalysts and their catalytic performance, present paper describes an *operando* Raman-GC study of alumina-supported MoVNbO and MoVNbTeO catalysts during partial oxidation of propane to acrylic acid.

---

[*] Corresponding author.
E-mail address: miguel.banares@csic.es (M.A. Bañares).

0926-860X/$ – see front matter © 2011 Elsevier B.V. All rights reserved.
doi:10.1016/j.apcata.2011.08.002

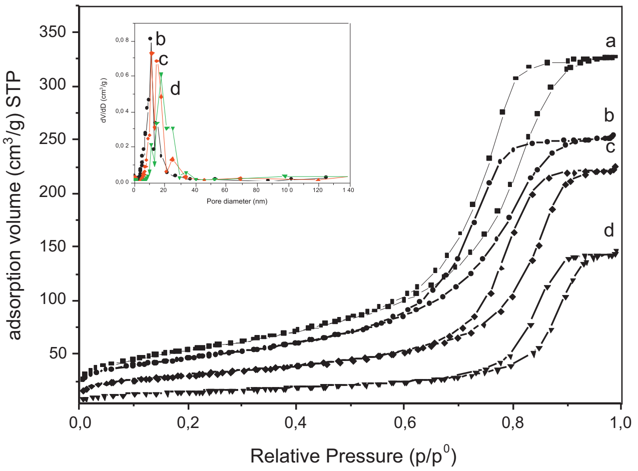

Fig. 1. Nitrogen adsorption–desorption isotherms of the (a) γ-Al_2O_3, (b) $4Mo_5V_4Nb_1$, (c) $8Mo_5V_4Nb_1$ and (d) $12Mo_5V_4Nb_1$ catalysts. Corresponding pore size distribution plots are show in the inset.

2. Experimental

2.1. Catalysts preparation

Alumina-supported catalysts containing Mo–V–Nb–(Te)–O were prepared by impregnation of γ-Al_2O_3 (Sasol Puralox SCCa 5/200, 193 m^2/g) with surface coverages varying from 4 to 12 metal atoms/nm^2 with aqueous solutions of ammonium heptamolybdate tetrahydrate $(NH_4)_6Mo_7O_{24}4H_2O$; (Sigma–Aldrich), NH_4VO_3 (Sigma–Aldrich), an aqueous solution of ammonium niobium soluble complex (Niobium Products) and telluric acid (Sigma–Aldrich). The slurry was introduced into a rotary evaporator at 80 °C and a reduced pressure of 10–40 mm Hg. The excess of water was evaporated while stirring at 80 °C; the remaining solid was then dried at 120 °C for 24 h and finally calcined at 600 °C for 2 h in air. The calcination was performed with a heating rate of 5 °C/min. The samples are named as $xMo_5V_4Nb_1$ or $xMo_5V_4Nb_{0.5}Te_{0.5}$, where "x" indicates the number of metal atoms per nm^2 of alumina support. Mo/V molar ratio was fixed at 5/4 whereas that for Mo/Nb, at 5. As a reference, the dispersion limit ("monolayer" coverage) of molybdenum, vanadium, niobium and tellurium oxide species on alumina is reached at ca. 6, 8 and 8 atoms/nm^2, respectively [19,20].

2.2. Characterization and operando experiments

The bulk elemental composition of catalysts was examined by inductively coupled plasma (ICP). The chemical analyses of the catalysts were carried out by inductively coupled plasma atomic emission spectroscopy (ICP-AES) using a Perkin–Elmer Optima 3300 DV spectrometer. The X-ray photoelectron spectra (XPS) were obtained with a VG Escalab 200R spectrometer equipped with a hemispherical electron analyzer and a MgKα ($h.\nu$ = 1254.6 eV, 1 eV = 1.6302 × 10^{-19} J) X-ray source, powered at 120 W. The contamination C_s line was selected as the kinetic energies reference, at a value of 284.6 eV. Wagner sensibility factors were used in order to quantify the different elements on the surface. Peaks were considered to be combinations of Gaussian and Lorentzian functions in a 80/20 ratio, working with a Shirley type baseline background subtraction by using XPS Peak Fit software. An estimated error of ±0.1 eV can be assumed for all measurements.

Powder X-ray diffraction (XRD) patterns of the samples were recorded on a Seifert 3000 diffractometer using Ni-filtered CuKα radiation ((= 0.15418 nm) and a graphite monochromator. Working conditions were 40 kV, 30 mA, and scanning rate of 2°/min for Bragg's angles 2θ from 5 to 70°. Analysis of the diffraction peaks was done with the computer program X'Pert HighScore Plus version 2.2a (2.2.1). Surface areas of the catalysts were measured from the adsorption isotherms of N_2 at −196 °C using the BET method ($0.05 < P/P_o < 0.27$) in a Micromeritics ASAP-2000 apparatus. The samples were previously degassed under helium flow at 140 °C for 2 h.

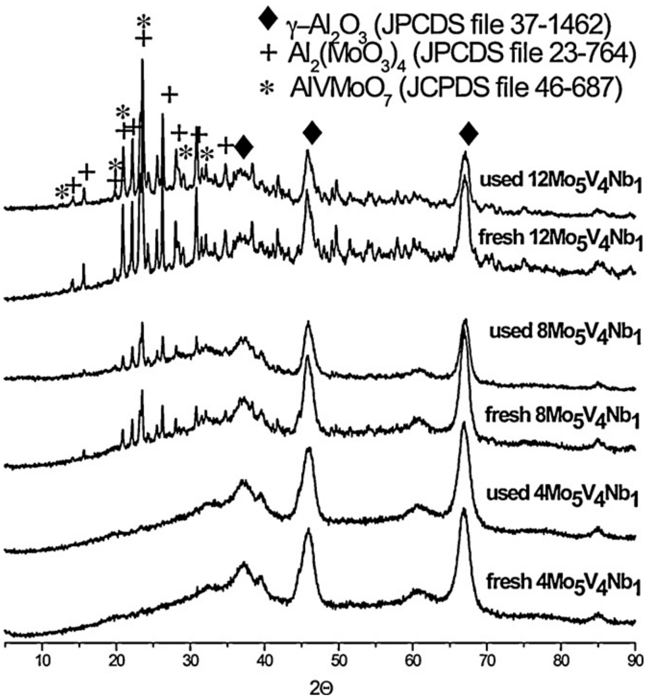

Fig. 2. XRD patters of $4Mo_5V_4Nb_1$, $8Mo_5V_4Nb_1$ and $12Mo_5V_4Nb_1$ catalysts.

Raman spectra were run with a Renishaw Micro-Raman System 1000 equipped with a cooled CCD detector and a holographic super-Notch filter to remove the elastic scattering. Wavenumber calibration of the spectrograph was checked daily using the Si line at 520 cm^{-1}. The samples were excited with the 488 nm line. The *in situ* laser Raman spectroscopy studies were carried out using an *operando* cell (Linkam) in which samples are heated in synthetic air flow (50 ml/min). The *operando* Raman experiments were obtained under reaction conditions in a home-made reaction cell [24]. It was made using quartz tubing connected to optical quality quartz. So, it was possible to make a fixed-bed catalytic reactor with walls that are optically appropriate for Raman spectroscopy. The laser power on the sample was kept very low (below 9 mW) to prevent local heating at the spot of spectral acquisition, which would have made the spectra not representative of the catalyst bed. As a consequence, the signal-to-noise ratio is low and acquisition time was adjusted to compensate (30 scans of 5 s). The activity in the *operando* reaction cell was measured with an on-line gas chromatograph, a Varian CP-3800 system equipped with a Porapak^{TM} Q and molecular sieve 5 Å column, fitted to TCD and FID detectors using an automatic sampling valve (VALCO). The correctness of the analytical determinations was checked for each test by verification that the carbon balance (based on the propane converted) was within the cumulative mean error of the determinations (±10%). To prevent participation of homogeneous reactivity, the reactor was designed to minimize gas-phase activation of propane by minimizing void volume. Tests were made using 0.2 g of sample with particle dimensions in the 0.25–0.125 mm range. The feed flow rate was fixed at 4800 h^{-1} (STP) gas hourly space velocity (GHSV). The reaction mixture consisted of 12.5 mol% C_3H_8, 20.4 mol% O_2, 15.9 mol% steam and 51.2 mol% He, and the flow rate was held constant at 40 ml/min.

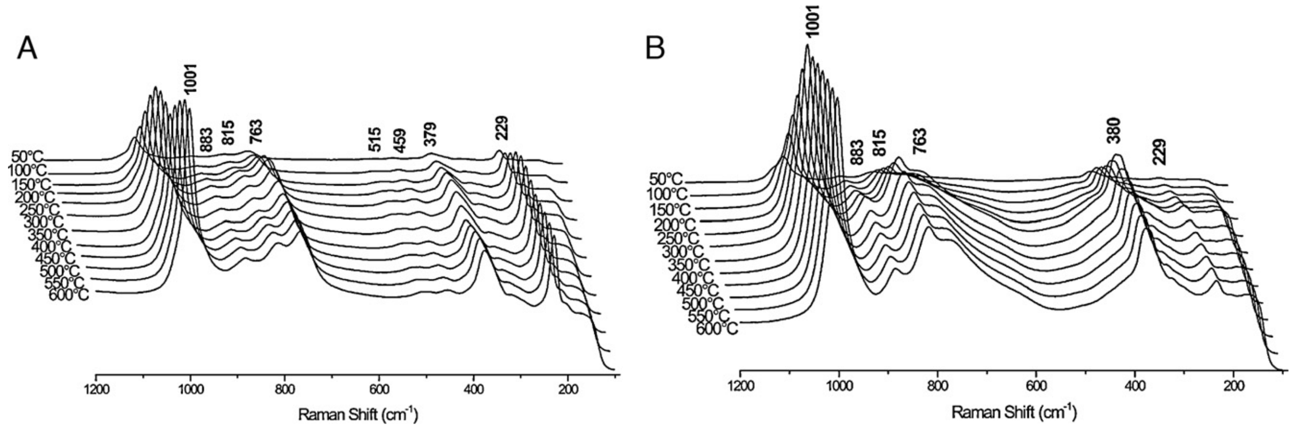

Fig. 3. *In situ* Raman spectra of (A) $4Mo_5V_4Nb_1$ and (B) $12Mo_5V_4Nb_1$ precursors under synthetic air atmosphere.

Table 1
Textural properties of catalysts.

Catalyst	Loading Mo + V + Nb (atoms/nm)	BET surface area (m^2/g)	Pore diameter (nm)	((Mo + V)/Al) ICP[a]	((Mo + V)/Al)) XPS[b]
$4Mo_5V_4Nb_1$	4	165	11	0.34	0.075
$8Mo_5V_4Nb_1$	8	110	16	0.48	0.586
$12Mo_5V_4Nb_1$	12	54	18	0.76	2.16

[a] Determined by ICP.
[b] Surface atomic ratios calculated from XPS data.

Table 2
Binding energies (eV) obtained by XPS.

	Fresh			Used		
Catalysts	V ($2p_{3/2}$)	Mo ($3d_{5/2}$)	Nb ($3d_{5/2}$)	V ($2p_{3/2}$)	Mo ($3d_{5/2}$)	Nb ($3d_{5/2}$)
$4Mo_5V_4Nb_1$	517.4 (89)[a] 516.1 (11)[b]	232.8 (85)[c] 231.7 (15)[d]	207.1	516.7 (100)[a]	232.7 (65)[c] 231.7 (35)[d]	207.1
$8Mo_5V_4Nb_1$	517.6 (94)[a] 516.3 (6)[b]	232.9 (90)[c] 231.7 (10)[d]	207.1	517.5 (100)[a]	232.8 (78)[c] 231.7 (22)[d]	207.1
$12Mo_5V_4Nb_1$	517.5 (100)[a]	232.9 (90)[c] 231.8 (10)[d]	207.3	517.5 (100)[a]	232.8 (84)[c] 231.7 (16)[d]	207.1

In parenthesis are peak percentages, [a] V^{5+} $2p_{3/2}$, [b] V^{4+} $2p_{3/2}$, [c] Mo^{6+} $3d_{5/2}$, [d] Mo^{5+} $3d_{5/2}$, [e] Nb^{5+} $3d_{5/2}$.

The *operando* reactor performance was benchmarked vs. conventional fixed-bed reactor, the reactants were feed with the same reaction feed system and the reaction products were analysed in the same GC system that was used for the *operando* Raman cell. The conventional cylindrical fixed-bed reactor (7 mm ID) was made of quartz too. The axial temperature profile was monitored by a thermocouple sliding inside the catalytic bed. In this case we used the same amount of catalyst with the same mesh and flows than those used during the *operando* experiments.

3. Results and discussion

3.1. MoVNbO supported catalysts

The BET surface area values of the samples are listed in Table 1. As expected, BET area decreases with total Mo + V + Nb coverage. In line with most supported oxides, BET area values drop dramatically above dispersion limit loading (ca. 8 atoms/nm^2), 12Mo5V4Nb1 BET area decreases to 54 m^2/g.

Fig. 1 shows the nitrogen adsorption–desorption isotherms, that represent a type IV isotherm according to the BDDT classification [25], with a hysteresis loop of type H1, indicating that these materials present a high mesoporosity. The hysteresis loop shifted

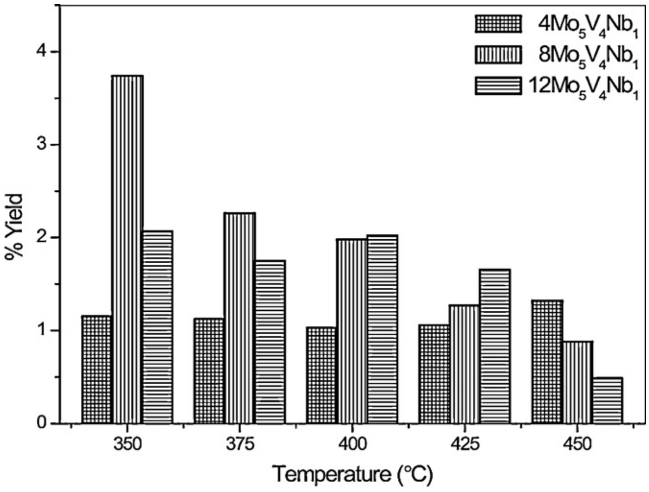

Fig. 4. Yield to acrylic acid during *operando* Raman-GC study during the selective oxidation of propane on $4Mo_5V_4Nb_1$, $8Mo_5V_4Nb_1$ and $12Mo_5V_4Nb_1$ catalysts. Reaction conditions: $C_3H_8/O_2/H_2O/He = 12.5/20.4/15.9/51.2$; 4800 h^{-1}; 0.2 g of catalyst.

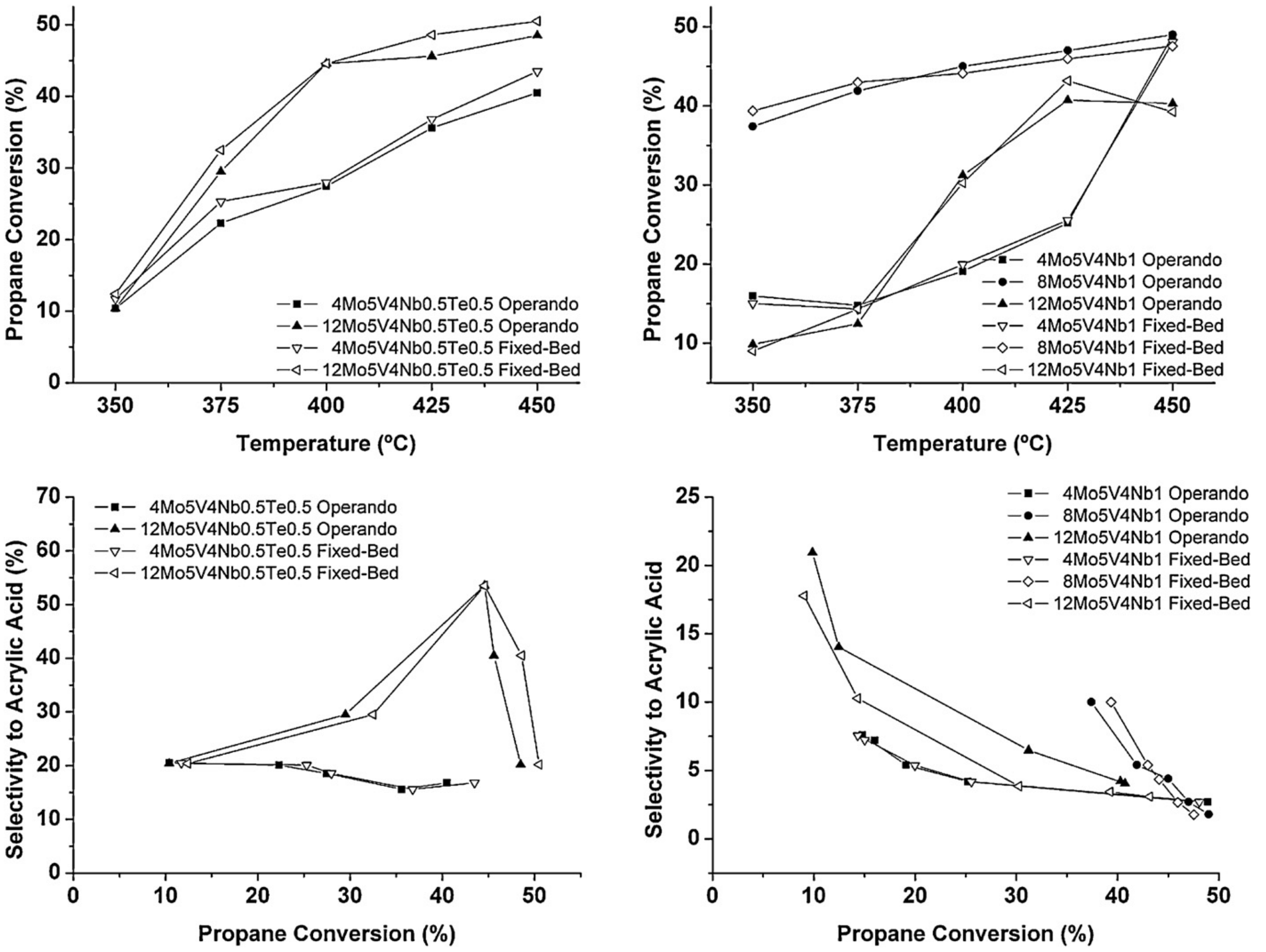

Fig. 5. Propane conversion vs. temperature and vs. selectivity to acrylic acid obtained for several catalysts in the conventional fixed bed reactor and in the operand reactor. Reaction conditions: $C_3H_8/O_2/H_2O/He = 12.5/20.4/15.9/51.2$; $4800\,h^{-1}$; 0.2 g of catalyst.

towards higher relative pressure, which reflects an increase in average pore size (see insert in Fig. 1 and Table 1). In order to have an idea about the composition at the surface, the (Mo + V)/Al ratios have been calculated by ICP and by XPS, and the results are included in Table 1. The Mo + V coverage on the surface, as determined by XPS, remains linear with bulk ICP loading trend, however, the XPS signal grows significantly faster than the bulk ratio, which indicates a high degree of coverage of alumina support. This makes sense since the dispersion limits for MoO_x and VO_x species on alumina support, understood as the maximum surface loading of oxide units that remain dispersed, with no crystalline V_2O_5 and/or MoO_3, have been calculated to be close to 8 atoms of Mo and/or V [26]. It is interesting to underline that pore diameter increases as total oxide coverage is increased (Table 1), from 12 nm in the $4Mo_5V_4Nb_1$ catalyst to 18 nm for $12Mo_5V_4Nb_1$ sample. Such increase in mesoporosity must be related with the supported oxide Mo–V–Nb–O structures, As has been described before [27,28] it is possible to prepare mesoporous bulk Mo–V–O oxides, in this case, a layer of mesoporous oxide structure has been obtained over an alumina support.

The XRD patterns for fresh and used catalysts are shown in Fig. 2. All the samples exhibit the diffraction pattern of alumina support (JPCDS file 37-1462). The sample with lowest coverage (fresh and aged) exhibits no other diffraction pattern. Crystalline Al–Mo–O and Al–Mo–V–O phases become increasingly visible as coverage increases; thus, alumina support interacts with the Mo–V–Nb–O phases. No XRD lines due to crystalline MoO_3 or V_2O_5 oxides are detected for any sample. No significant changes are observed in these patterns before and after the catalytic tests.

The binding energies of Mo $3d_{5/2}$, V $2p_{3/2}$ and Nb $3d_{5/2}$ peaks for 4Mo4V4Nb1 sample are shown in Table 2. For Mo region, the spin-orbit splitting between the $Mo3d_{5/2}$ and $Mo3d_{3/2}$ signals was fixed to 3.1 eV and the intensity ratio was set to 0.67. Deconvolution of the spectra of fresh and used catalysts indicate the presence of two different Mo species, whose binding energies correspond to Mo^{5+} and Mo^{6+} species [29–31]. The population of the reduced Mo^{5+} species increases in the catalyst after use in catalytic tests.

The V 2p spectra for the fresh sample exhibit two components: one at higher binding energy, near 517.4 eV, associated with V^{5+} species [32], and another at lower energy, near 516.1 eV, related with the presence of V^{4+} species [33]. After reaction, only one component associated with V^{5+} species is detected, thus, during propane oxidation some changes in the overall oxidation states of vanadium and molybdenum species are detected by the changes in the binding energies. Binding energies of Nb3d levels for fresh and used samples are characteristic of Nb^{5+} species [34,35].

Raman spectra provide additional information about the structure of the MoVNbO-based catalysts due to its sensitivity to nanosized crystalline domains that do not generate diffraction patterns. Fig. 3 shows the Raman spectra during calcination in

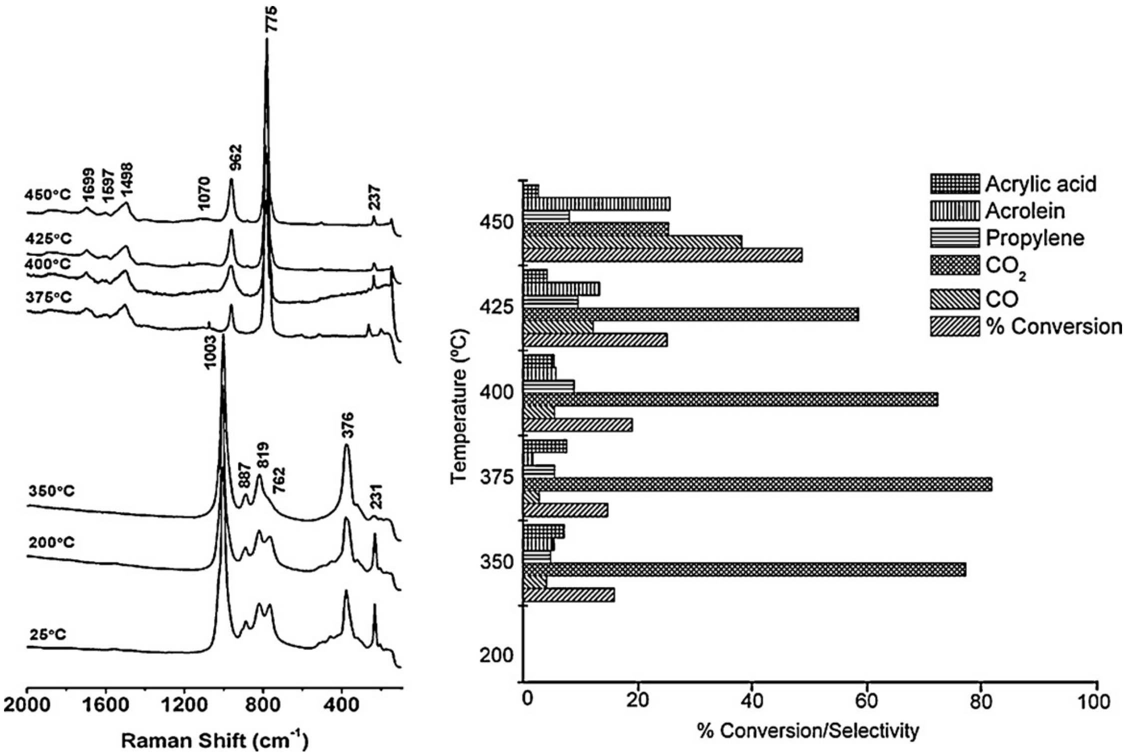

Fig. 6. *Operando* Raman-GC spectra during the selective oxidation of propane on $4Mo_5V_4Nb_1$; (left), Raman spectra during reaction at the temperature indicated; (right), simultaneous activity/selectivity data obtained during Raman spectra acquisition. Reaction conditions: $C_3H_8/O_2/H_2O/He = 12.5/20.4/15.9/51.2$; 4800 h^{-1}; 0.2 g of catalyst.

synthetic air for samples with the lowest (Fig. 3A) and the highest (Fig. 3B) coverages. In all the cases, a strong signal near 990–1030 cm^{-1} is detected. Such band is characteristic of the stretching modes of Mo═O and/or V═O bonds, suggesting the presence of surface MoO_x and/or VO_x species [20,36]. Also, in that region, some bands can be assigned to vibrations of Mo–O–V bonds [37–39]. The Raman band near 883 cm^{-1} is characteristic of Mo_5O_{14} structures [40,41]. This band is more intense for the sample with higher coverage.

Raman bands near 815 and 380 cm^{-1} are more intense in Fig. 3B, for the sample with the highest coverage; such Raman bands have been reported for Mo–V-oxide based catalysts [37,42] and belong

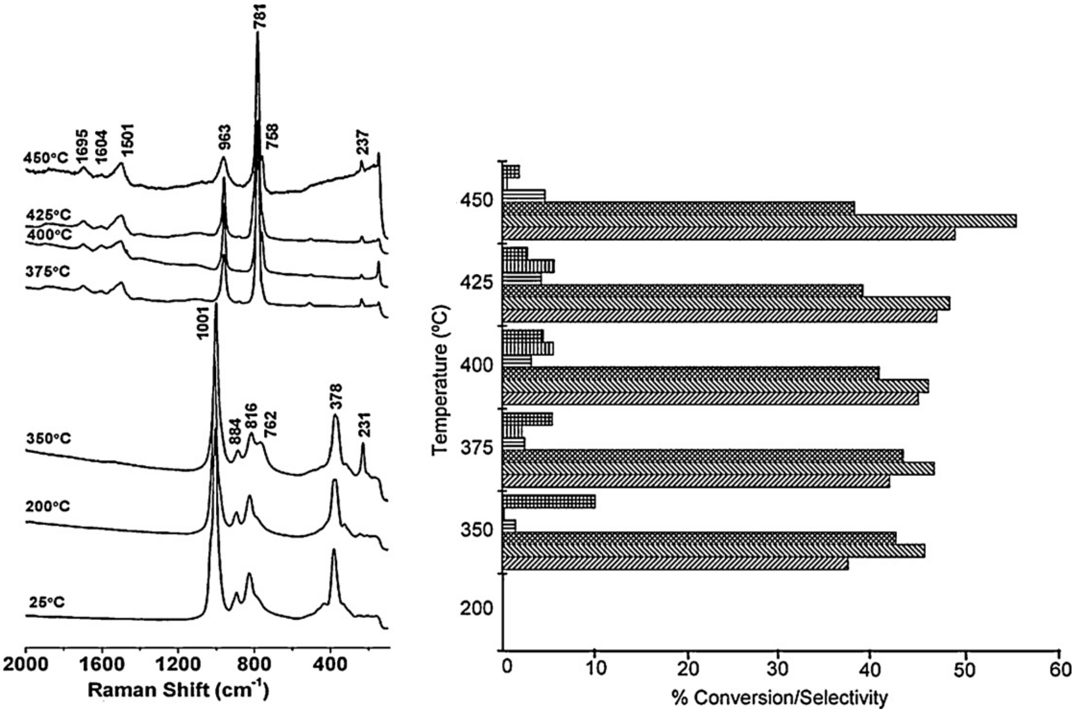

Fig. 7. *Operando* Raman-GC spectra during the selective oxidation of propane on $8Mo_5V_4Nb_1$; (left), Raman spectra during reaction at the temperature indicated; (right), simultaneous activity/selectivity data obtained during Raman spectra acquisition. $C_3H_8/O_2/H_2O/He = 12.5/20.4/15.9/51.2$; 4800 h^{-1}; 0.2 g of catalyst.

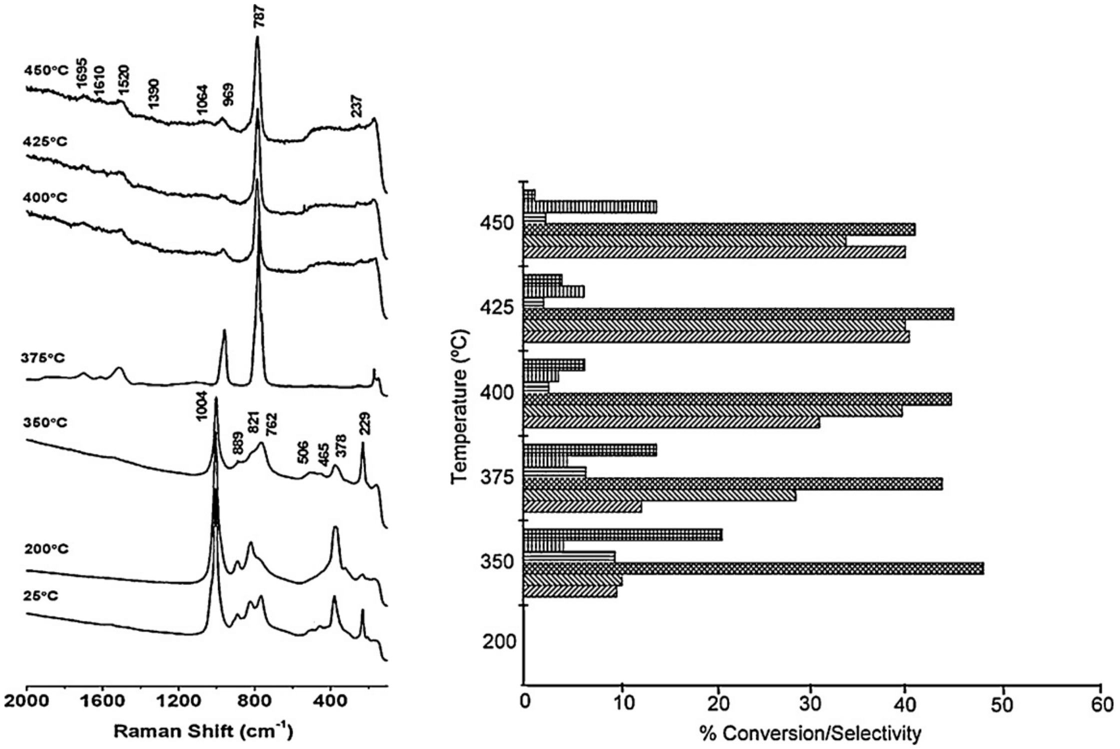

Fig. 8. *Operando* Raman-GC spectra during the selective oxidation of propane on $12Mo_5V_4Nb_1$; (left), Raman spectra during reaction at the temperature indicated; (right), simultaneous activity/selectivity data obtained during Raman spectra acquisition. $C_3H_8/O_2/H_2O/He = 12.5/20.4/15.9/51.2$; 4800 h^{-1}; 0.2 g of catalyst.

to a Mo–V–O phase. It makes sense that by increasing the coverage, the presence of some interactions between molybdenum and vanadium species is detected. On the contrary, Raman bands near 770 and 230 cm^{-1}, are more intense for the sample with lower coverage, such bands are related to an $AlVMoO_7$ structure [42]. The intensity of these bands increases with temperature, indicating that the thermal treatment enhances the interactions of the supported Mo and V species with the alumina support.

Fig. 4 shows yields to acrylic acid at different temperatures vs. coverage on alumina; coverage close to the monolayer (8 atoms/nm^2) affords better performances. Sample with lower coverage performs worse than the others, this sample do not reach dispersion limit coverage, and thus do not form bulk mixed oxide phases that appear necessary for this process. Only, at the highest temperature, it outperforms the other two catalysts, but the yield is significantly lower than that achieved by the other catalysts at significantly lower temperatures. It should be noted that the highest yields are obtained at the lowest temperature (350 °C) whereas there is a significant drop in performance at 375 °C and above.

3.2. *Operando study*

The *operando* Raman-GC study during propane ammoxidation was performed under reaction conditions in a home-made *operando* reaction cell that was described previously [24], which was designed in our laboratory [43]. Essentially, it is a fixed-bed catalytic reactor with walls that are optically appropriate for *in situ* Raman spectroscopy. Thus, such reactor allows obtaining the Raman spectrum of the catalysts and genuine catalytic data. Fig. 5 shows the results obtained for several catalysts at different temperatures in the *operando*-reactor and also in the conventional fixed bed reactor; it can be observed how the activity/selectivity obtained in both reactors is essentially the same. These results are in accordance with previous papers in which was described that the activity values obtained in the *operando* reactor for other reactions [24,42]. Thus, the catalytic and structural study will be based on the *operando* reactor data.

Figs. 6–8 show the catalytic results obtained during propane oxidation and the Raman spectra obtained during the *operando* study. In all the cases, when the temperature reaction is increased up to 375 °C, the shape of the spectra changes drastically. Bellow that temperature, Raman bands near 815 and 380 cm^{-1} assigned to Mo–V–O structures and bands near 1000 cm^{-1} assigned to MoO_x and/or VO_x dominate the spectra. In addition, Raman bands near 760 and 230, assigned to $AlVMoO_7$ structure can be detected and the Raman band near 880 cm^{-1} assigned to Mo_5O_{14}-type structure. Conversely, Raman bands near 960, 780 and 237 cm^{-1} dominate the spectra when reaction temperature reaches 375 °C; such Raman

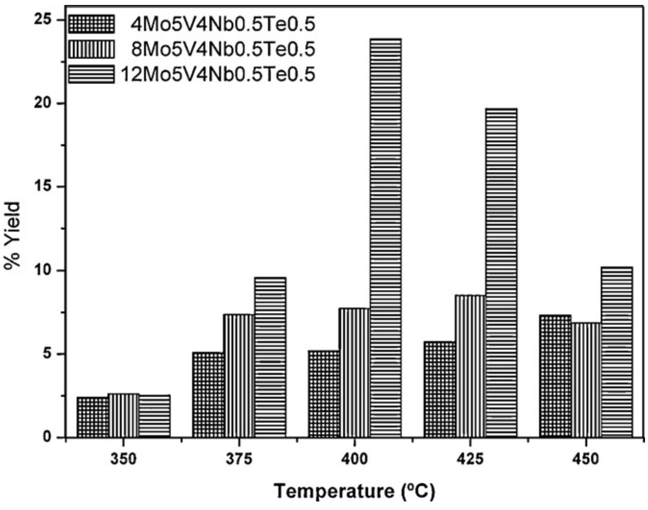

Fig. 9. Yield to acrylic acid during the selective oxidation of propane on $4Mo_5V_4Nb_{0.5}Te_{0.5}$, $8Mo_5V_4Nb_{0.5}Te_{0.5}$ and $12Mo_5V_4Nb_{0.5}Te_{0.5}$ catalysts. Reaction conditions: $C_3H_8/O_2/H_2O/He = 12.5/20.4/15.9/51.2$; 4800 h^{-1}; 0.2 g of catalyst.

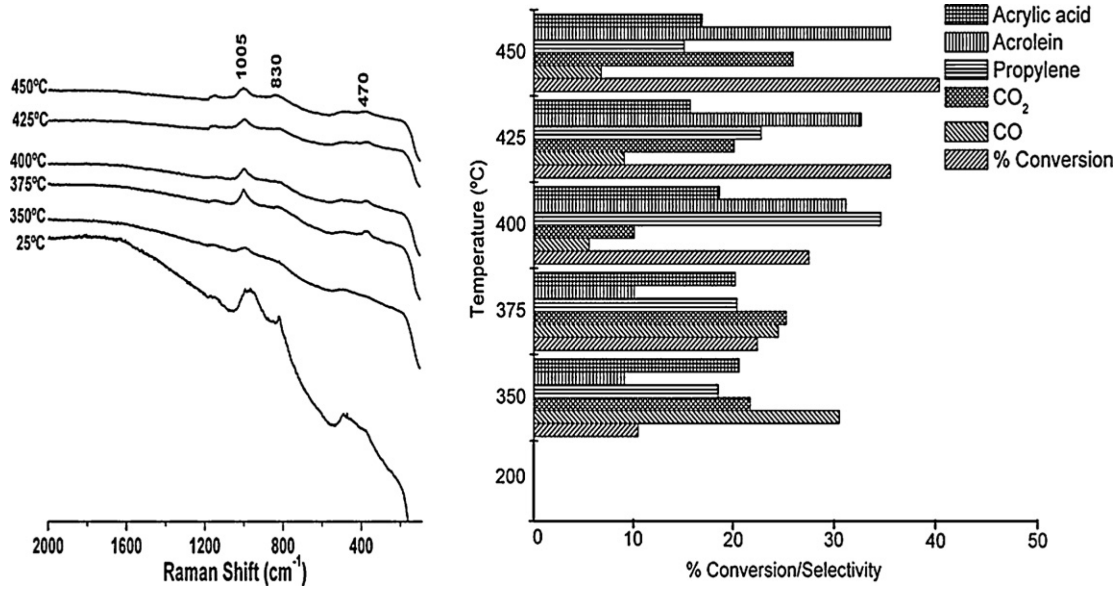

Fig. 10. *Operando* Raman-GC spectra during the selective oxidation of propane on $4Mo_5V_4Nb_{0.5}Te_{0.5}$; (left), Raman spectra during reaction at the temperature indicated; (right), simultaneous activity/selectivity data obtained during Raman spectra acquisition. Reaction conditions: $C_3H_8/O_2/H_2O/He = 12.5/20.4/15.9/51.2$; 4800 h^{-1}; 0.2 g of catalyst.

bands are indicative of a α-MoO_3 with some minor amounts of vanadium species [20,44]. The amount of such MoO_3 structure is not very high since no diffraction pattern for a similar structure has been detected, but its bands dominate the Raman spectra since this phase possesses very high Raman section. XRD analyses uncover the presence of Mo–V–O and Mo–V–Al–O phases, which are not seen by Raman spectra, probably due to their lower Raman scattering section; thus, the spectra are dominated by the distorted oxide-like structure. Raman spectra uncover important changes at the nanometer scale during reaction, which are not told by XRD. All catalysts exhibit significant changes at 375 °C that reflect significant changes on the structures of the supported oxides. Such changes appear consistent with those underlined by the XPS BE values of used catalysts. These indicate that Mo species reduce whereas vanadium species are oxidized. These results are in line with previous paper with similar catalytic systems. The selectivity to partial oxidation products is higher when mixed phases form (e.g., Mo–V–O, V–P–O or Sb–V–O), typically in their rutile phase; on the contrary, the distribution of product shifts to non-selective oxidation products (CO_x) if segregated V_2O_5, Sb_2O_3 and/or MoO_3 oxides form.

In addition to monitoring changes occurring in the nanoscaled Nb–Mo–V–O structures during propane oxidation, *operando* Raman experiments evidence the formation of coke since bands appear in the region 1200–1650 cm^{-1} are attributed to graphite-like carbon deposits assigned to surface layers of sp^2 carbon species [45–48], indicative that coke structures are appearing on the surface of catalysts.

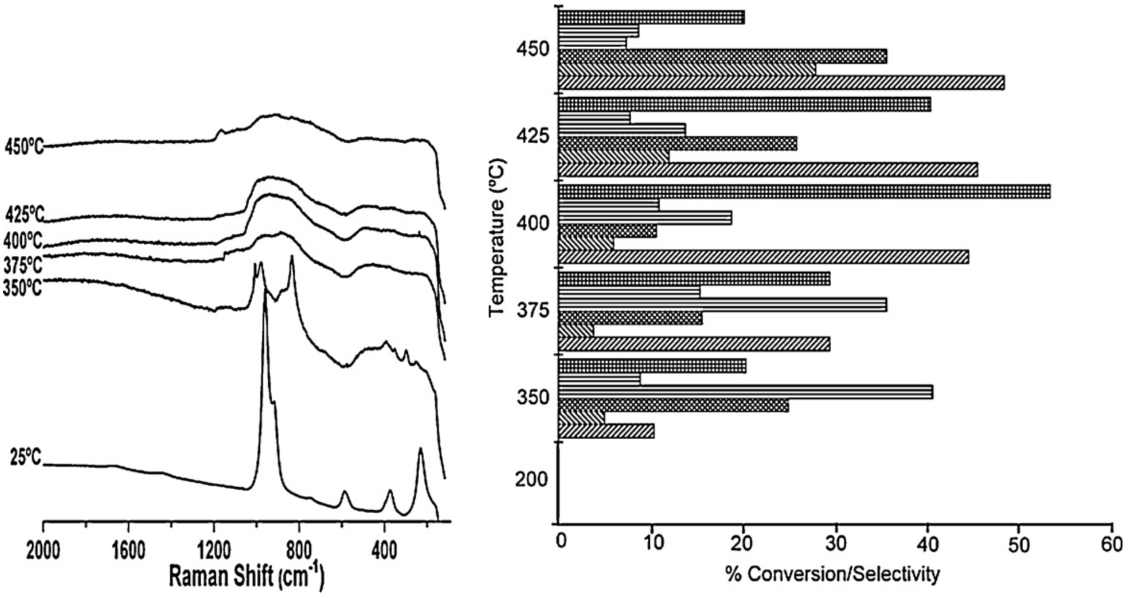

Fig. 11. *Operando* Raman-GC spectra during the selective oxidation of propane on $12Mo_5V_4Nb_{0.5}Te_{0.5}$; (left), Raman spectra during reaction at the temperature indicated; (right), simultaneous activity/selectivity data obtained during Raman spectra acquisition. Reaction conditions: $C_3H_8/O_2/H_2O/He = 12.5/20.4/15.9/51.2$; 4800 h^{-1}; 0.2 g of catalyst.

3.3. Effect of tellurium

In order to improve the catalytic behaviour of these materials three more catalysts were prepared by adding tellurium as dopant, with the formulation $Mo_5V_4Nb_{0.5}Te_{0.5}$. The XRD of fresh and used Te-containing catalysts is shown in Additional supporting information. Fig. 9 shows the yields to acrylic acid vs. reaction temperature. The catalytic behaviour is markedly different to that delivered by the tellurium-free series (Fig. 4). In this case the yield to acrylic acid is higher, especially for the sample with the highest coverage, which delivers ca. 25% acrylic acid yield. In order to assess the nature of the structural changes that tellurium induces during reaction, the *operando* study was performed with 12 $Mo_5V_4Nb_{0.5}Te_{0.5}$, that is the one that presented the highest acrylic acid yields. As a reference, this is compared to the catalysts with lowest coverage.

Fig. 10 shows the *operando* study of the catalysts with lowest coverage ($4Mo_5V_4Nb_{0.5}Te_{0.5}$), which possess a BET surface area of 159 m^2/g, very similar to the 165 m^2/g of its tellurium-free counterpart (Table 1). The selectivity to acrylic acid for $4Mo_5V_4Nb_{0.5}Te_{0.5}$ (Fig. 10) increases at all the temperatures with respect to the catalyst without tellurium (Fig. 6); acrylic acid is not the main product, though. This comparison shows that a small amount of tellurium changes both the structure and the activity of the catalysts. Unlike the tellurium-free series, the Raman bands of mixed Mo–V–O, Mo–V–Al–O phases are not evident at low reaction temperature, and the Raman bands of MoO_3 phase at high reaction temperature are not apparent either. This suggests that tellurium doping has a dramatic effect on the structures of mixed Mo–V oxides. Which is evidenced by a broad Raman signal in the 800–1000 cm^{-1} [15,49] range; this is indicative that tellurium induces the presence of highly distorted rutile structures. Such distorted rutile structures are important for obtaining active and selective catalysts; probably due to the structural flexibility under reaction conditions of rutile phases, which can accommodate cation vacancies enhancing the possibilities for the adsorption of the reactants [15,50]. Such an effect prevents the formation of MoO_3 oxide, which is detrimental for acrylic acid production, and minimizes the formation of coke at high reaction temperatures. As a consequence, the selectivity to acrylic acid increases, but in this case, with such a low coverage, the amount of active phase is quite low and acrylic acid is not the main reaction product.

The *operando* Raman-GC study was also performed with a catalyst with higher coverage, $12Mo_5V_4Nb_{0.5}Te_{0.5}$, with a BET surface area of 74 m^2/g. In this case tendency is the same, since the formation of MoO_3 and the build-up of coke deposits is not observed in our experimental conditions (Fig. 11). In this case, Raman bands in the 900–1020 cm^{-1} range and the Raman bands near 820 and 370 cm^{-1} of dispersed oxides are apparent during reaction at 350 °C. Such dispersed oxide structures blend into distorted rutile structure phases as the reaction temperature increases (375–450 °C). Such rutile structures exhibit a broad Raman signal near 800 cm^{-1}, This band is stronger than for the lowest-coverage catalyst (Fig. 8), which indicates that the amount of rutile (active phase) is higher, in line with its higher yield to acrylic acid.

4. Conclusions

Operando Raman-GC studies show changes occurring at the nanometer scale in the surface of catalysts during reaction, although no changes were detected by XRD. The catalytic results obtained at the *operando* reactor are benchmarked vs. conventional fixed-bed reactors, exhibiting essentially the same activity/selectivity, within experimental error. The *operando* study of MoVNb catalysts shows that at low reaction temperature mixed Al–V–Mo and V–Mo oxide phases dominate the surface of the catalysts. The entanglement between Mo and V ions, along with those from alumina support, appears critical for an efficient oxidation reaction. When reaction temperature reaches 375 °C, the catalyst structure transforms, losing molybdenum oxide phases rich in V and Al. These transform into α-MoO_3 crystallites distorted by a small fraction of V ions, which results in a less efficient system. These data underline the direct involvement of mixed Mo–V–(Al)–O phases on propane oxidation. In addition, incipient coke formation becomes apparent when the selectivity to acrylic acid decreases. Tellurium doping generates highly distorted rutile structures during reaction, capable of inhibiting the formation of α-MoO_3 crystallites under reaction conditions, and improving the catalytic performance of these catalysts, reaching an acrylic acid yield of ca. 25% at 400 °C.

Acknowledgements

The Ministry of Science and Innovation (Spain) funded this study under project CTQ2008-04261/PPQ. R.L.M. thanks MAEC-AECID (Spain) for his pre-doctoral fellowship and Elizabeth Rojas García for her help with catalytic tests. The authors express their thanks to Olaf Torno (Sasol Germany GmbH) for providing alumina support.

Appendix A. Supplementary data

Supplementary data associated with this article can be found, in the online version, at doi:10.1016/j.apcata.2011.08.002.

References

[1] N.R. Shiju, V.V. Guliants, Appl. Catal. A 356 (2009) 1–17.
[2] W. Ueda, M. Sadakane, H. Ogihara, Catal. Today 132 (2008) 2–8.
[3] J.M. López Nieto, Top. Catal. 41 (2006) 3–15.
[4] G. Tsilomelekis, S. Boghosian, Catal. Today 158 (2010) 146–155.
[5] V.V. Guliants, R. Bhandari, J.N. Al-Saeedi, V.K. Vasudevan, R.S. Soman, M.O. Guerrero-Pérez, M.A. Bañares, Appl. Catal. A 274 (2004) 123–132.
[6] L. Yuan, V.V. Guliants, M.A. Bañares, S.J. Khatib, Top. Catal. 49 (2008) 268–280.
[7] M.O. Guerrero-Pérez, M.C. Herrera, I. Malpartida, M.A. Larrubia, L.J. Alemany, Catal. Today 133–135 (2008) 919–924.
[8] P. Botella, B. Solsona, J.M. López-Nieto, P. Concepción, J.L. Jordá, M.T. Doménech-Carbó, Catal. Today 158 (2010) 162–169.
[9] M. Dieterle, G. Mestl, J. Jäger, Y. Uchida, H. Hibst, R. Schlögl, J. Mol. Catal. A: Chem. 174 (2001) 169–185.
[10] R. Schlögl, A. Knop-Gericke, M. Hävecker, U. Wild, D. Frickel, T. Ressler, R.E. Jentoft, J. Wienold, G. Mestl, A. Blume, O. Timpe, Y. Uchida, Top. Catal. 15 (2001) 219–228.
[11] M. Roussel, S. Barama, A. Löfberg, S. Al-Sayari, K. Karim, E. Bordes-Richard, Catal. Today 141 (2009) 288–293.
[12] M.A. Bañares, Catal. Today 100 (2005) 71–77.
[13] B.M. Weckhuysen, Chem. Commun. 97 (2002) 12–13.
[14] B.M. Weckhuysen, Angew. Chem. Int. Ed. 48 (2009) 4910–4943.
[15] M.O. Guerrero-Pérez, M.A. Bañares, Chem. Commun. 12 (2002) 1292–1293.
[16] M.O. Guerrero-Pérez, M.A. Bañares, Catal. Today 113 (2006) 48–57.
[17] M.V. Martínez-Huerta, G. Deo, J.L.G. Fierro, M.A. Bañares, J. Phys. Chem. C 112 (2008) 11441–11447.
[18] M.A. Bañares, M.O. Guerrero-Pérez, J.L.G. Fierro, G.G. Cortez, J. Mater. Chem. 12 (2002) 3337–3342.
[19] M.A. Bañares, I.E. Wachs, J. Raman Spectrosc. 33 (2002) 359–380.
[20] M.A. Bañares, G. Mestl, Adv. Catal. 52 (2009) 43–128.
[21] S.M. Bennici, B.M. Vogelaar, T.A. Nijhuis, B.M. Weckhuysen, Angew. Chem. Int. Ed. 46 (2007) 5412–5416.
[22] R. López-Medina, J.L.G. Fierro, M.O. Guerrero-Pérez, M.A. Bañares, Appl. Catal. A 375 (2010) 55–62.
[23] R. López-Medina, H. Golinska, M. Ziolek, M.O. Guerrero-Pérez, M.A. Bañares, Catal. Today 158 (2010) 139–145.
[24] M.O. Guerrero-Pérez, M.A. Bañares, Catal. Today 96 (2004) 265–272.
[25] S. Brunauer, P.H. Emmett, E. Teller, J. Am. Chem. Soc. 60 (1938) 309–319.
[26] J.M. Jehng, A.M. Turek, I.E. Wachs, Appl. Catal., A 83 (1992) 179–200.
[27] L. Yuan, V.V. Guliants, J. Porous Mater. 16 (2009) 613–622.
[28] L. Yuan, V.V. Guliants, J. Mater. Sci. 43 (2008) 6278–6284.
[29] W. Grünert, A.Y. Stakheev, R. Feldhaus, K. Anders, E.S. Shpiro, K.M. Minachev, J. Phys. Chem. 95 (1991) 1323–1328.
[30] S. Andonova, C. Vladov, B. Pawelec, I. Shtereva, G. Tyuliev, S. Damyanova, L. Petrov, Appl. Catal. A 328 (2007) 201–209.
[31] D. Gazzoli, F. Prinetto, M.C. Campa, A. Cimino, G. Ghiotti, V. Indovina, M. Valigi, Surf. Interface Anal. 22 (1994) 398–402.
[32] H. Watanabe, Y. Koyasu, Appl. Catal. A 194–195 (2000) 479–485.

[33] M.O. Guerrero-Pérez, M.C. Herrera, I. Malpartida, M.A. Larrubia, L.J. Alemany, Catal. Today 118 (2006) 360–365.
[34] M. Roussel, M. Bouchard, E. Bordes-Richard, K. Karim, S. Al-Sayari, Catal. Today 99 (2005) 77–87.
[35] V.V. Atuchin, I.E. Kalabin, V.G. Kesler, N.V. Pervukhina, J. Electron. Spectrosc. Relat. Phenom. 142 (2005) 129–134.
[36] M.O. Guerrero-Pérez, M.C. Herrera, I. Malpartida, M.A. Larrubia, L.J. Alemany, M.A. Bañares, Catal. Today 126 (2007) 177–183.
[37] M.O. Guerrero-Pérez, L.J. Alemany, Appl. Catal. A 341 (2008) 119–126.
[38] N. Haddad, E. Bordes-Richard, L. Hilaire, A. Barama, Catal. Today 126 (2007) 256–263.
[39] N. Haddad, E. Bordes-Richard, A. Barama, Catal. Today 142 (2009) 215–219.
[40] G. Mestl, J. Raman Spectrosc. 33 (2002) 333–347.
[41] G. Mestl, Ch. Linsmeier, R. Gottschall, M. Dieterle, J. Find, D. Herein, J. Jäger, Y. Uchida, R. Schlögl, J. Mol. Catal. A: Chem. 162 (2000) 463–492.
[42] M.A. Bañares, S.J. Khatib, Catal. Today 96 (2004) 251–257.
[43] M.V. Martínez-Huerta, PhD Dissertation, Universidad Autónoma de Madrid, 2001.
[44] S. Damyanova, L.M. Gomez, M.A. Bañares, J.L.G. Fierro, Chem. Mater. 12 (2000) 501–510.
[45] G. Mul, M.A. Bañares, G.G. Cortéz, B. van der Linden, S.J. Khatibb, J.A. Moulijna, Phys. Chem. Chem. Phys. 5 (2003) 4378–4383.
[46] F. Cavani, N. Ballarini, M. Cimini, F. Trifirò, M. Bañares, M.O. Guerrero-Pérez, Catal. Today 112 (2006) 12–16.
[47] E. Tuinstra, J.L. Koenig, J. Chem. Phys. 53 (1970) 1126–1130.
[48] S.J. Tinnemans, M.H.F. Kox, T.A. Nijhuis, T. Visser, B.M. Weckhuysen, Phys. Chem. Chem. Phys. 7 (2005) 211–216.
[49] M.O. Guerrero-Pérez, J.L.G. Fierro, M.A. Vicente, M.A. Bañares, Chem. Mater. 19 (2007) 6621–6628.
[50] A.R. Landa-Cánovas, F.J. García-García, S. Hansen, Catal. Today 158 (2010) 156–161.